SCIENTIFIC REP⚙RTS

Chaotic Resonance in Typical Routes to Chaos in the Izhikevich Neuron Model

Sou Nobukawa [1], Haruhiko Nishimura[2] & Teruya Yamanishi[3]

Chaotic resonance (CR), in which a system responds to a weak signal through the effects of chaotic activities, is a known function of chaos in neural systems. The current belief suggests that chaotic states are induced by different routes to chaos in spiking neural systems. However, few studies have compared the efficiency of signal responses in CR across the different chaotic states in spiking neural systems. We focused herein on the Izhikevich neuron model, comparing the characteristics of CR in the chaotic states arising through the period-doubling or tangent bifurcation routes. We found that the signal response in CR had a unimodal maximum with respect to the stability of chaotic orbits in the tested chaotic states. Furthermore, the efficiency of signal responses at the edge of chaos became especially high as a result of synchronization between the input signal and the periodic component in chaotic spiking activity.

Stochastic resonance (SR) is a phenomenon in which the presence of noise helps a non-linear system amplify a weak (under-barrier) signal[1, 2]. In the past few decades, a considerable number of studies about SR in biological systems has been conducted[3–6]. More recently, studies of SR have been conducted using neural systems which possess various kinds of spiking patterns and complex physiological network structures. For example, Perc and Marhl examined frequency locking due to additive noise in the resting state near the bifurcation point leading to the chaotic-burst spiking state[7]. Nobukawa and Nishimura demonstrated that spike-timing-dependent plasticity may be made efficient through the effect of SR in neural systems composed of three types of spiking patterns: regular spiking (RS), intrinsically bursting (IB) and chattering (CH)[8]. Wang et al. showed that multiple SRs, in which coherence measures of signal responses are maximized at multiple levels of noise strength, was observed in scale-free spiking neural networks with synaptic delay and pacemaker neurons[9]. Yilmaz et al. demonstrated that the presence of electrical synapses can enhance the efficiency of signal transmission in SR in the scale-free spiking neural network when including electrical and chemical synapses[10]. Teramae et al.[11] showed that the spontaneous activity widely observed in actual cortical neural networks can be reproduced when incorporating SR. They noted this in the spiking neural network in which the strength of excitatory synaptic weights obeys a non-Gaussian, long-tailed, typically log-normal distribution. Also, many kinds of synchronization phenomena which are not restricted to SR, such as synchronization transition and chimera states, have been widely found in scale-free complex and physiological spiking neural networks with both delay and multiple structures[12–17].

Furthermore, several studies have analyzed synchronization phenomena typified by chaos synchronization and phase synchronization among neurons, and with external input signals, in spiking neural networks with chaotic spiking activity[18–21]. Among these synchronization phenomena, it has been known that fluctuating activities in deterministic chaos cause a phenomenon that is similar to SR. In the corresponding phenomenon, called chaotic resonance (CR), the system responds to the weak input signal through engaging the effects of intrinsic chaotic activities under conditions in which no additive noise exists[2, 22]. Initially, CR was investigated using a one-dimensional cubic map and Chua's circuit[23–27], though more recently neural systems have been utilized[28–33]. In a previous study, we discovered that the signal response of CR in a spiking neural system has a unimodal maximum with respect to the degree of stability for chaotic orbits, as quantified by the maximum Lyapunov exponent[34]. That is, the appropriate chaotic behavior leads to the generation of spikes (i.e., exceeds the threshold) not at specific times, but at varying scattered times for each trial, as input signals. This frequency distribution of these spike timings against the input signal becomes congruent with the shape of the input signal.

[1]Department of Computer Science, Chiba Institute of Technology, 2-17-1 Tsudanuma, Narashino, 275-0016, Japan. [2]Graduate School of Applied Informatics, University of Hyogo, 7–1–28 Chuo-ku, Kobe, 650–8588, Japan. [3]Department of Management Information Science, Fukui University of Technology, 3-6-1 Gakuen, Fukui, 910-8505, Japan. Correspondence and requests for materials should be addressed to S.N. (email: nobukawa@cs.it-chiba.ac.jp)

A considerable number of studies have been conducted on chaos and bifurcation in spiking neural systems, generating model systems that include the Hodgkin-Huxley, FitzHugh-Nagumo, and Hindmarsh-Rose models[35]. In particular, the Izhikevich neuron model, as a hybrid spiking neuron model, combines a continuous spike generation mechanism and a discontinuous after-spike resetting process; thus, the model can induce many kinds of bifurcations, and reproduce almost all spiking activities observed in actual neural systems simply by tuning a few parameters[36]. In addition, the variety of reproduced spiking patterns is high in comparison with other spiking neuron models[37].

The hybrid spiking neuron model is one of the piecewise-smooth dynamical systems, in which dynamics are switched according to the state of the system[38]. Saito and colleagues have conducted chaos/bifurcation analysis and circuit implementation against piecewise-constant dynamical systems, and piecewise-linear dynamical systems, as simplified versions of the piecewise-smooth dynamical system[39–41]. In particular, Tsubone *et al.* proposed a systematic method to predict parameter regions for chaotic states using an analytical approach in the piecewise-constant dynamical system[41]. While in general, piecewise-smooth dynamical systems include non-linear terms similar to those seen in the Izhikevich neuron model, an approach for evaluating Lyapunov exponents and characteristic multipliers that considers the saltation matrix[38] through simulations against exhaustive parameter sets is needed. On considering this approach, it is clear that this model has various kinds of bifurcations and routes to chaos when under the effect of the state-dependent jump in the resetting process[34, 42–44]. However, the signal responses of CR have not been evaluated in chaotic states produced through different routes.

In our preliminary work, we confirmed the presence of CR in chaotic states induced by different routes (i.e., the periodic-doubling bifurcation route and intermittency route to chaos) in the Izhikevich neuron model[45]. In this paper, we build on our previous work and evaluate the signal responses in CR, and compare the characteristics across these chaotic states through two methods. We first examine the dependence of the signal response on the maximum Lyapunov exponent; then we identify the resonant zone in the parameter space of the applied signal frequency/amplitude.

Materials and Methods

Izhikevich neuron model.
The Izhikevich neuron model[36, 37] is a two-dimensional ordinary differential equation of the form

$$\dot{v} = 0.04v^2 + 5v + 140 - u + I, \tag{1}$$

$$\dot{u} = a(bv - u), \tag{2}$$

and with auxiliary after-spike resetting

$$\text{if } v \geq 30[\text{mV}], \text{ then} \begin{cases} v \leftarrow c \\ u \leftarrow u + d. \end{cases} \tag{3}$$

Here, v and u represent the membrane potential of a neuron and the membrane recovery variable, respectively.

We extended Eq. (1) using a weak periodic signal $I_{ext}(t)$ as follows:

$$\dot{v} = 0.04v^2 + 5v + 140 - u + I + I_{ext}(t), \tag{4}$$

in which we adopted $I_{ext}(t) = A\sin(2\pi f_0 t)$. Note that the sinusoidal signal was utilized merely as a typical example of a signal in a neural system.

Evaluation indices.
Indices for evaluation of chaos and bifurcation. To quantify the chaotic activity in the Izhikevich neuron model, the Lyapunov exponent with a saltation matrix is utilized. On a system with a continuous trajectory between the i-th and the $(i+1)$-th spiking times, $(t_i \leq t \leq t_{i+1})$, the variational equations (1) and (2) are defined as follows:

$$\dot{\Phi}_{i+1}(t, t_i) = J(v, u, t)\Phi_{i+1}(t, t_i), \tag{5}$$

$$\Phi_{i+1}(t_i, t_i) = E, \tag{6}$$

where Φ, J, and E indicate the state transition matrix, the Jacobian matrix, and a unit matrix, respectively. At $t = t_i$, the saltation matrix is given by

$$S_i = \begin{bmatrix} \dfrac{\dot{v}^+}{\dot{v}^-} & 0 \\ \dfrac{\dot{u}^+ - \dot{u}^-}{\dot{v}^-} & 1 \end{bmatrix}, \tag{7}$$

In the above, (v^-, u^-) and (v^+, u^+) represent the values of (v, u) before and after spiking, respectively. In case spikes arise in the range $[T^k:T^{k+1}]$ [ms], $\Phi^k(T^{k+1}, T^k)$ $(k = 0, 1, \ldots, N-1)$[43] can be expressed as

$$\Phi^k(T^{k+1}, T^k) = \Phi_{i+1}(T^{k+1}, t_i)S_i\Phi_i(t_i, t_{i-1})\cdots S_2\Phi_2(t_2, t_1)S_1\Phi_1(t_1, T^k). \tag{8}$$

Based on the eigenvalues l_j^k $(j = 1, 2)$ of $\Phi^k(T^{k+1}, T^k)$, the Lyapunov spectrum λ_j is calculated by
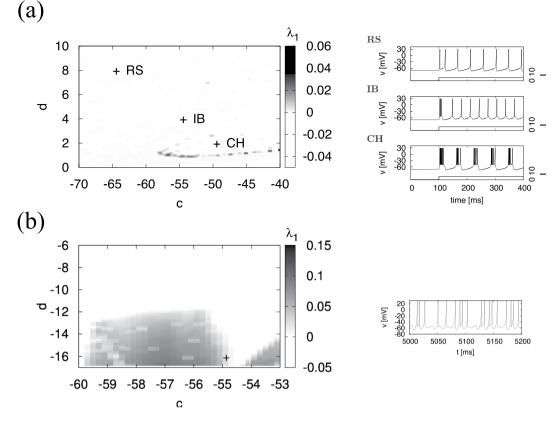
Figure 1. Dependence of maximum Lyapunov exponent λ_1 on parameters c and d. (**a**) Region around the parameter sets for regular spiking (RS), intrinsically bursting (IB), and chattering (CH). The symbols of $(+)$ indicate the parameter sets for RS and IB, CH ($a = 0.02$, $b = 0.2$, $I = 10$). The chaotic states ($\lambda_1 > 0$) exist in $-59 \lesssim c \lesssim -40$, $d \approx 1.0$. (**b**) Region around the parameter set proposed by Izhikevich for chaotic spiking. The symbols of $(+)$ indicate the parameter set for chaotic spiking ($a = 0.2$, $b = 2$, $I = -99$). The chaotic states ($\lambda_1 > 0$) exist in $d \lesssim -13$.

$$\lambda_j = \frac{1}{T^N - T^0} \sum_{k=0}^{N-1} \log(|l_j^k|). \tag{9}$$

In our simulation, we set $T^{k+1} - T^k$ as the time required for 20 spikes ($i = 20$). We set 1000 [ms] as the maximum value in case $T^{k+1} - T^k$ lasts for 1000 [ms] before 20 spikes occur.

In order to conduct bifurcation analysis in the system with a state-dependent jump, we set a Poincaré section $\Psi(v = 30)$. The dynamics of system behavior on Ψ are indicated by the Poincaré map $u_{i+1} = \psi(u_i)$ where u_i is the value of u on Ψ. In the literature[42], the stability of a fixed point $u_0 = \psi(u_{l-1})\cdots\psi(u_1)\psi(u_0) \equiv \psi^l(u_0)$ ($l = 1, 2, \cdots$) is evaluated by

$$\mu^l = \frac{\partial \psi^l}{\partial \mathbf{u}_0} = (0 \quad 1) \begin{pmatrix} 0 & 0 \\ -\dot{v}/\dot{u} & 1 \end{pmatrix} \Phi(t_l, t_0) \begin{pmatrix} 0 \\ 1 \end{pmatrix}. \tag{10}$$

Here, $\mathbf{u}_0 = (v_0, u_0)$ indicates the initial value of orbit $\mathbf{u} = (v, u)$ at $t = t_0$. $|\mu^l| < 1|$, $\mu^l = -1$, and $\mu^l = 1$ represent the stable condition, period-doubling bifurcation, and tangent bifurcation, respectively.

Indices for evaluation of signal response. We calculated the timing of the spikes against signal $I_{ext}(t)$ by using a cycle histogram $F(\tilde{t})$[33]. $F(\tilde{t})$ was a histogram of firing counts at $t_k \bmod (T_0)$ ($k = 1, 2, \ldots$) against signal $I_{ext}(\tilde{t})$ with period $T_0 = (1/f_0), 0 \leq \tilde{t} \leq T_0$. For example, for $T_0 = 10$, if the spike times were $t_k = 2, 6, 12, 16, 26$, the values of $t_k \bmod (T_0)$ were 2, 6, 2, 6, 6. The cycle histogram then became $F(2) = 2$ and $F(6) = 3$.

To quantify the signal response, we used the following index of Eqs (11) and (14). The mutual correlation $C(\tau)$ between the cycle histogram $F(\tilde{t})$ of the neuron spikes and the signal $I_{ext}(\tilde{t})$ is given by
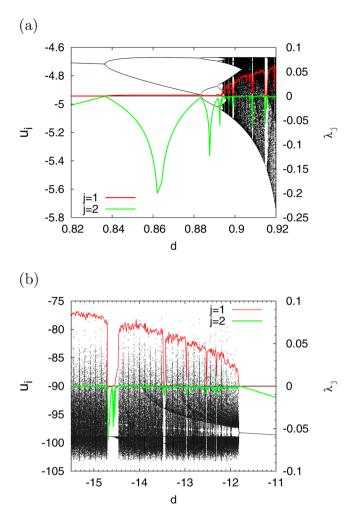
$$C(\tau) = \frac{C_{IF}(\tau)}{\sqrt{C_{II}C_{FF}}} \tag{11}$$

(a)

(b)

Figure 2. Bifurcation diagram of u_i on Poincaré section Ψ and Lyapunov exponents λ_j as function of parameter d ($j = 1, 2$). (**a**) Period-doubling bifurcation case (called region #1) ($a = 0.02$, $b = 0.2$, $c = -55$, $I = 10$). The period-doubling bifurcation ($\mu^l = -1$) arises at $d \approx 0.8348, 0.8828, 0.8916, 0.894$, and the chaotic state ($\lambda_1 > 0$, $\lambda_2 = 0$) appears $d \gtrsim 0.894$ through a period-doubling bifurcation route. (**b**) Tangent bifurcation case (called region #2) ($a = 0.2$, $b = 2$, $c = -56$, $I = -99$). The tangent bifurcation ($\mu^l = 1$) arises at $d \approx -11.9$ and the chaotic state ($\lambda_1 > 0$, $\lambda_2 = 0$) appears $d \lesssim -11.9$ through the intermittency route.

$$C_{IF}(\tau) = \langle (I_{ext}(\tilde{t} + \tau) - \langle I_{ext}(\tilde{t}) \rangle)(F(\tilde{t}) - \langle F(\tilde{t}) \rangle) \rangle \tag{12}$$

$$C_{II} = \langle (I_{ext}(\tilde{t}) - \langle I_{ext}(\tilde{t}) \rangle)^2 \rangle \tag{13}$$

$$C_{FF} = \langle (F(\tilde{t}) - \langle F(\tilde{t}) \rangle)^2 \rangle \tag{14}$$

For the time delay factor τ, we checked $\max_\tau C(\tau)$, i.e., the largest $C(\tau)$ between $0 \leq \tau \leq T_0$.

Results

Parameter region for evaluating signal responses. Initially, we determined the parameter regions where the chaotic state is produced. The left panels of Fig. 1(a) and (b) show the dependences of the maximum Lyapunov exponent λ_1 on parameters c and d in the region around parameter sets for the spiking patterns of RS, IB, and CH (see the right part of Fig. 1(a)) and the region around the parameter set proposed by Izhikevich for chaotic spiking (see the right part of Fig. 1(b)), respectively. The chaotic states ($\lambda_1 > 0$) exist in $-59 \lesssim c \lesssim -40$, $d \approx 1.0$ in the former case, and $d \lesssim -13$ in the latter case. As the parameter regions for evaluating CR, we chose $0.82 \leq d \leq 0.92$ in the former region (called region #1 below), and $-15.5 \leq d \leq -11$ in the latter region (called region #2 below). Figure 2 depicts the bifurcation diagram of u_i on Poincaré section Ψ (black dot) and Lyapunov exponents (red dotted ($j = 1$) and green dashed ($j = 2$) lines) as a function of parameter d in region #1 case (a) and region #2 case (b). In Fig. 2(a), the period-doubling bifurcation ($\mu^l = -1$) arises at $d \approx 0.8348, 0.8828, 0.8916$, 0.894, and the chaotic state ($\lambda_1 > 0$, $\lambda_2 = 0$) appears $d \gtrsim 0.894$. Hence, the period-doubling bifurcation route to
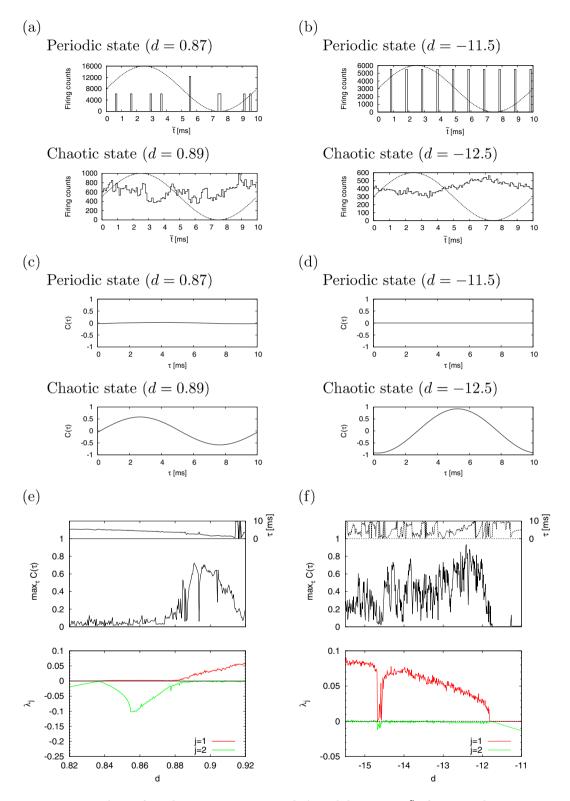
Figure 3. Dependence of signal response on parameter d. The cycle histogram $F(\tilde{t})$ of neuron spikes is congruent with the signal $I_{ext}(\tilde{t})$ in chaotic regions, i.e., chaotic resonance (CR) arises. (**a**) Cycle histogram $F(\tilde{t})$ in the periodic state (upper) and the chaotic state (lower) in the case of region #1. ($a = 0.02$, $b = 0.2$, $c = -55$, $I = 10$). (**b**) The case of region #2. ($a = 0.2$, $b = 2$, $I = -99$). (**c**) Mutual correlation $C(\tau)$ between the cycle histogram $F(\tilde{t})$ of the neuron spikes and the signal $I_{ext}(\tilde{t})$ in the case of region #1. (**d**) The case of region #2. (**e**) $\max_{\tau} C(\tau)$ (upper) and Lyapunov exponent λ_j ($j = 1, 2$) (lower) as a function of parameter d in the case of region #1. (**f**) The case of region #2.
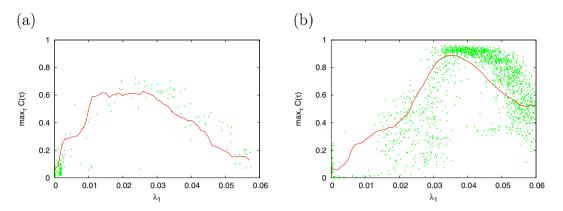
(a)

(b)

Figure 4. Scatter plot between $\max_\tau C(\tau)$ and λ_1 obtained in Fig. 3 (red dotted line: mean value of $\max_\tau C(\tau)$ in bin λ_1 with window $\Delta\lambda_1 = 0.001$). Signal response in CR has a unimodal maximum with respect to the stability for chaotic orbits represented by λ_1, (**a**) Region #1. (**b**) Region #2.
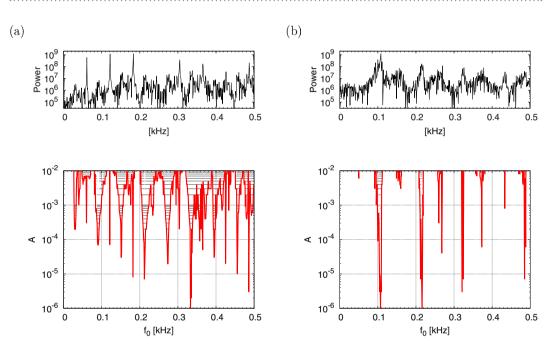
(a)

(b)

Figure 5. Power spectrum of the time series of $v(t)$ in the signal-free condition (upper). Resonant frequency f_0/amplitude A zone and points ($\max_\tau C(\tau) > 0.5$), indicated by the red line and black points, respectively, in the signal-adapted condition (lower). The resonant zones have a tendency to distribute near the peaks for the power spectrum in the signal-free condition. (**a**) Edge of the chaotic state in region #1 ($d = 0.896$). (**b**) Edge of the chaotic state in region #2 ($d = -12.0$).

chaos exists in this region. However, as shown in Fig. 2(b), the tangent bifurcation ($\mu^l = 1$) arises at $d \approx -11.9$ and the chaotic state $d \lesssim -11.9$ ($\lambda_1 > 0$, $\lambda_2 = 0$) appears. This chaotic state produced by tangent bifurcation indicates the alternating laminar and turbulent modes of intermittency chaos in a general way[46]; this dynamic was demonstrated in our previous work[34]. That is, the intermittency route to chaos exists in this region.

Signal response in chaotic resonance. In the above mentioned chaotic parameter regions #1 and #2, we evaluated the response against a weak signal ($A = 10^{-2}$, $f_0 = 0.1$). To begin with, we compared the cycle histograms $F(\tilde{t})$ between periodic and chaotic states. As shown in Fig. 3, in the cases of both region #1 (a) and region #2 (b), $F(\tilde{t})$ in the periodic state (solid line) does not fit $I_{ext}(\tilde{t})$ (dotted line) because the periodic response against $I_{ext}(\tilde{t})$ induces growth in its values at specific bins. On the other hand, $F(\tilde{t})$ in the chaotic state fits $I_{ext}(\tilde{t})$ according to a chaotic response with scatter timing against $I_{ext}(t)$. This tendency can also be observed in their $C(\tau)$ as shown in Fig. 3(c) and (d). That is, $C(\tau)$ becomes approximately 0 in the periodic state, but $C(\tau)$ exhibits a sinusoidal shape in the chaotic state. In the following evaluations, we use $\max_\tau C(\tau)$ to characterize the signal response, because the sinusoidal shape of $C(\tau)$ with period T_0 can be identified by amplitude and lag corresponding to $\max_\tau C(\tau)$ and its τ value. Furthermore, this signal response is evaluated using $\max_\tau C(\tau)$ and λ_1. Figure 3(e) and (f) show the

dependence of $\max_\tau C(\tau)$ (upper) and λ_j ($j = 1, 2$) (lower) on parameter d in regions #1 and #2, respectively. In region #1 (Fig. 3(a)), the neuron exhibits the periodic spiking ($\lambda_1 \approx 0$, $\lambda_2 < 0$) in $0.82 \lesssim d \lesssim 0.88$, and the chaotic spiking ($\lambda_1 > 0$, $\lambda_2 \approx 0$) in $0.88 \lesssim d \lesssim 0.92$. In the periodic spiking state, the value of $\max_\tau C(\tau)$ is less than 0.1; whereas in the chaotic spiking state, the value of $\max_\tau C(\tau)$ is higher in comparison with the periodic spiking state. In particular, at the $d \approx 0.89$ location around the bifurcation to chaos, called the edge of chaos[47] below, $\max_\tau C(\tau)$ has a peak value (≈ 0.8). This can be interpreted as CR arising in the chaotic region ($0.88 \lesssim d \lesssim 0.92$). In region #2 (Fig. 3(b)), the chaotic spiking state ($\lambda_1 > 0$, $\lambda_2 \approx 0$) arises in $-15.5 \lesssim d \lesssim -12$ and $\max_\tau C(\tau)$, and is a high value due to the effect of this chaotic spiking state. Also, the value of $\max_\tau C(\tau)$ indicates a similar tendency for region #1 (Fig. 3(a)), i.e., at the $d \approx -12.3$ location around the bifurcation to chaos, $\max_\tau C(\tau)$ has a peak value (≈ 0.9).

Furthermore, Fig. 4(a) and (b) show the scatter plots between $\max_\tau C(\tau)$ and λ_1 obtained in Fig. 3 in the cases of region #1 and region #2, respectively. The red dotted line indicates the mean value of $\max_\tau C(\tau)$ in bin λ_1 with window $\Delta \lambda_1 = 0.001$. From these results, in both regions, $\max_\tau C(\tau)$ peaks at the appropriate value of $\max_\tau C(\tau)$ ($\max_\tau C(\tau) \approx 0.7$ at $\lambda_1 \approx 0.03$ in region #1 and $\max_\tau C(\tau) \approx 0.9$ at $\lambda_1 \approx 0.04$ in region #2). The points for this appropriate value for λ_1 correspond to the points representing the edge of chaos in Fig. 3. That is, the signal response in CR has a unimodal maximum with respect to the stability for chaotic orbits represented by λ_1, and this peak is localized at the edge of chaos.

Signal sensitivity in the edge of chaos region.

In the edge of chaos, i.e., the chaotic state near the bifurcation point, the power spectrum for the time series of system behavior has several peaks. In the periodic bifurcation route to chaos, the trajectory is restricted to the narrow space around the multiple-periodic trajectory before the points at the bifurcation to chaos. Therefore, the power spectrum of the chaotic state inherits the peaks from the power spectrum of the multiple-periodic state, while in the intermittency route to chaos, the laminar state dominates in the time series of system behavior. Hence, the power spectrum has peaks near the frequency components of the laminar state. The upper panels of Fig. 5 show the power spectrum of $v(t)$ under the signal-free condition in the edge of chaos in region #1 (a) ($d = 0.896$) and #2 (b) ($d = -12.0$). For the reasons described above, the power spectrum has several peaks. Furthermore, as shown in the lower panels of Fig. 5, resonant frequency/amplitude zones and points ($\max_\tau C(\tau) > 0.5$) indicated by the red line and black points, respectively, in the signal-adapted condition. Here, its frequency f_0 corresponds to the horizontal line of the upper panels of Fig. 5. From this result, the resonant zones have a tendency to distribute near the peaks for the power spectrum in the signal-free condition. This is especially significant with the weaker signal amplitude regions.

Discussion and Conclusions

We showed herein two distinct routes to chaos, the period-doubling bifurcation route and the intermittency route, by using the Lyapunov exponent with a saltation matrix and index for stability of a fixed point on the Poincaré section. Furthermore, under the condition of receiving input from a weak periodic signal, the enhancement of the signal response by the effect of chaotic spikes (chaotic resonance) was confirmed in the chaotic regions induced by the above routes to chaos. Specifically, in both chaotic regions, the signal response in CR had a unimodal maximum with respect to the stability for chaotic orbits represented by λ_1. Thus, it can be interpreted that the instability of the chaotic orbit in CR plays a role of the noise strength in SR.

Furthermore, we have confirmed that the peak of the signal response was located in the edge of chaos. There, we identified the periodic components in chaotic spiking activity as shown in Fig. 5. In the case of a relatively large signal strength, we found broadening of the signal frequency region in which the efficient signal response was high. On the other hand, in the case of a small signal strength, the region of high efficiency was restricted to the immediate neighborhoods of frequencies for the periodic components in chaotic spiking. This characteristic of signal response in relation to signal strength and frequency, called Arnold's tongue, is widely observed in synchronization phenomena[48]. Therefore, the high efficiency of signal responses in the edge of chaos could be interpreted as synchronization between the input signal and the periodic component in chaotic spiking activity.

In future work, we intend to evaluate the signal response in CR in large-sized spiking neural networks.

References

1. Benzi, R., Sutera, A. & Vulpiani, A. The mechanism of stochastic resonance. *Journal of Physics A: mathematical and general* **14**, L453 (1981).
2. Gammaitoni, L., Hänggi, P., Jung, P. & Marchesoni, F. Stochastic resonance. *Reviews of modern physics* **70**, 223–287 (1998).
3. Moss, F. & Wiesenfeld, K. The benefits of background noise. *Scientific American* **273**, 66–69 (1995).
4. Hänggi, P. Stochastic resonance in biology how noise can enhance detection of weak signals and help improve biological information processing. *ChemPhysChem* **3**, 285–290 (2002).
5. Mori, T. & Kai, S. Noise-induced entrainment and stochastic resonance in human brain waves. *Physical Review Letters* **88**, 218101 (2002).
6. McDonnell, M. D. & Ward, L. M. The benefits of noise in neural systems: bridging theory and experiment. *Nature Reviews Neuroscience* **12**, 415–426 (2011).
7. Perc, M. & Marhl, M. Amplification of information transfer in excitable systems that reside in a steady state near a bifurcation point to complex oscillatory behavior. *Physical Review E* **71**, 026229 (2005).
8. Nobukawa, S. & Nishimura, H. Enhancement of spike-timing-dependent plasticity in spiking neural systems with noise. *International journal of neural systems* **26**, 1550040 (2016).
9. Wang, Q., Perc, M., Duan, Z. & Chen, G. Delay-induced multiple stochastic resonances on scale-free neuronal networks. *Chaos: An Interdisciplinary Journal of Nonlinear Science* **19**, 023112 (2009).
10. Yilmaz, E., Uzuntarla, M., Ozer, M. & Perc, M. Stochastic resonance in hybrid scale-free neuronal networks. *Physica A: Statistical Mechanics and its Applications* **392**, 5735–5741 (2013).

11. Teramae, J.-n., Tsubo, Y. & Fukai, T. Optimal spike-based communication in excitable networks with strong-sparse and weak-dense links. *Scientific reports* **2**, 485 (2012).
12. Wang, Q., Duan, Z., Perc, M. & Chen, G. Synchronization transitions on small-world neuronal networks: Effects of information transmission delay and rewiring probability. *EPL (Europhysics Letters)* **83**, 50008 (2008).
13. Wang, Q., Perc, M., Duan, Z. & Chen, G. Synchronization transitions on scale-free neuronal networks due to finite information transmission delays. *Physical Review E* **80**, 026206 (2009).
14. Wang, Q., Chen, G. & Perc, M. Synchronous bursts on scale-free neuronal networks with attractive and repulsive coupling. *PLoS one* **6**, e15851 (2011).
15. Majhi, S., Perc, M. & Ghosh, D. Chimera states in uncoupled neurons induced by a multilayer structure. *Scientific Reports* **6** (2016).
16. Hizanidis, J., Kouvaris, N. E., Gorka, Z.-L., Daz-Guilera, A. & Antonopoulos, C. G. Chimera-like states in modular neural networks. *Scientific reports* **6** (2016).
17. Bera, B. K., Ghosh, D. & Banerjee, T. Imperfect traveling chimera states induced by local synaptic gradient coupling. *Physical Review E* **94**, 012215 (2016).
18. Yu, H. *et al.* Chaotic phase synchronization in small-world networks of bursting neurons. *Chaos: an interdisciplinary journal of nonlinear science* **21**, 013127 (2011).
19. Yu, H. *et al.* Chaotic phase synchronization in a modular neuronal network of small-world subnetworks. *Chaos: an Interdisciplinary Journal of Nonlinear Science* **21**, 043125 (2011).
20. Rehan, M., Hong, K.-S. & Aqil, M. Synchronization of multiple chaotic FitzHugh–Nagumo neurons with gap junctions under external electrical stimulation. *Neurocomputing* **74**, 3296–3304 (2011).
21. Ferrari, F. A., Viana, R. L., Lopes, S. R. & Stoop, R. Phase synchronization of coupled bursting neurons and the generalized Kuramoto model. *Neural Networks* **66**, 107–118 (2015).
22. Anishchenko, V. S., Astakhov, V., Neiman, A., Vadivasova, T. & Schimansky-Geier, L. *Nonlinear dynamics of chaotic and stochastic systems: tutorial and modern developments* (Springer Science & Business Media, 2007).
23. Carroll, T. & Pecora, L. Stochastic resonance and crises. *Physical review letters* **70**, 576–579 (1993).
24. Carroll, T. & Pecora, L. Stochastic resonance as a crisis in a period-doubled circuit. *Physical Review E* **47**, 3941–3949 (1993).
25. Crisanti, A., Falcioni, M., Paladin, G. & Vulpiani, A. Stochastic resonance in deterministic chaotic systems. *Journal of Physics A: Mathematical and General* **27**, 597–603 (1994).
26. Nicolis, G., Nicolis, C. & McKernan, D. Stochastic resonance in chaotic dynamics. *Journal of statistical physics* **70**, 125–139 (1993).
27. Sinha, S. & Chakrabarti, B. K. Deterministic stochastic resonance in a piecewise linear chaotic map. *Physical Review E* **58**, 8009–8012 (1998).
28. Nishimura, H., Katada, N. & Aihara, K. Coherent response in a chaotic neural network. *Neural Processing Letters* **12**, 49–58 (2000).
29. Nobukawa, S., Nishimura, H. & Katada, N. Chaotic resonance by chaotic attractors merging in discrete cubic map and chaotic neural network. *IEICE Trans. A* **95**, 357–366 (2012) (in Japanese).
30. Schweighofer, N. *et al.* Chaos may enhance information transmission in the inferior olive. *Proceedings of the National Academy of Sciences of the United States of America* **101**, 4655–4660 (2004).
31. Schweighofer, N., Lang, E. J. & Kawato, M. Role of the olivo-cerebellar complex in motor learning and control. *Front. Neural Circuits* **7**, 10–3389 (2013).
32. Tokuda, I. T., Han, C. E., Aihara, K., Kawato, M. & Schweighofer, N. The role of chaotic resonance in cerebellar learning. *Neural Networks* **23**, 836–842 (2010).
33. Nobukawa, S. & Nishimura, H. Chaotic resonance in coupled inferior olive neurons with the Llinás approach neuron model. *Neural Computation* **28**, 2505–2532 (2016).
34. Nobukawa, S., Nishimura, H., Yamanishi, T. & Liu, J.-Q. Analysis of chaotic resonance in Izhikevich neuron model. *PloS one* **10** (2015).
35. Rabinovich, M. I., Varona, P., Selverston, A. I. & Abarbanel, H. D. Dynamical principles in neuroscience. *Reviews of modern physics* **78**, 1213–1265 (2006).
36. Izhikevich, E. M. Simple model of spiking neurons. *IEEE Transactions on neural networks* **14**, 1569–1572 (2003).
37. Izhikevich, E. M. Which model to use for cortical spiking neurons? *IEEE transactions on neural networks* **15**, 1063–1070 (2004).
38. Bernardo, M., Budd, C., Champneys, A. R. & Kowalczyk, P. *Piecewise-smooth dynamical systems: theory and applications*, vol. 163 (Springer Science & Business Media, 2008).
39. Yotsuji, K. & Saito, T. Basic analysis of a hyperchaotic spiking circuit with impulsive switching. *Nonlinear Theory and Its Applications, IEICE* **5**, 535–544 (2014).
40. Kimura, K., Suzuki, S., Tsubone, T. & Saito, T. The cylinder manifold piecewise linear system: Analysis and implementation. *Nonlinear Theory and Its Applications, IEICE* **6**, 488–498 (2015).
41. Tsubone, T., Saito, T. & Inaba, N. Design of an analog chaos-generating circuit using piecewise-constant dynamics. *Progress of Theoretical and Experimental Physics* **2016**, 053A01 (2016).
42. Tamura, A., Ueta, T. & Tsuji, S. Bifurcation analysis of Izhikevich neuron model. *Dynamics of continuous, discrete and impulsive systems, Series A: mathematical analysis* **16**, 759–775 (2009).
43. Bizzarri, F., Brambilla, A. & Gajani, G. S. Lyapunov exponents computation for hybrid neurons. *Journal of computational neuroscience* **35**, 201–212 (2013).
44. Nobukawa, S., Nishimura, H., Yamanishi, T. & Liu, J.-Q. Chaotic states induced by resetting process in Izhikevich neuron model. *Journal of Artificial Intelligence and Soft Computing Research* **5**, 109–119 (2015).
45. Nobukawa, S., Nishimura, H., Yamanishi, T. & Liu, J.-Q. Evaluation of resonance phenomena in chaotic states through typical routes in Izhikevich neuron model. In *Proceedings of 2015 International Symposium on Nonlinear Theory and its Applications (NOLTA2015)*, 435–438 (IEICE, 2015).
46. Nagashima, H. & Baba, Y. Introduction to chaos: physics and mathematics of chaotic phenomena (CRC Press, 1998).
47. Langton, C. G. Computation at the edge of chaos: phase transitions and emergent computation. *Physica D: Nonlinear Phenomena* **42**, 12–37 (1990).
48. Pikovsky, A., Rosenblum, M. & Kurths, J. *Synchronization: a universal concept in nonlinear sciences*, vol. 12 (Cambridge university press, 2003).

Acknowledgements

Author Contributions

S.N., T.Y., and H.N. conceived the methods, S.N. conducted the experiments, S.N. and H.N. analyzed the results. All authors reviewed the manuscript.

Additional Information

Competing Interests: The authors declare that they have no competing interests.

Publisher's note: Springer Nature remains neutral with regard to jurisdictional claims in published maps and institutional affiliations.